Temperature-dependent quantum efficiency degradation of K-Cs-Sb bialkali antimonide photocathodes grown by a triple-element codeposition method

Zihao Ding,[1] Siddharth Karkare,[2] Jun Feng,[2] Daniele Filippetto,[2] Matthew Johnson,[2] Steve Virostek,[2] Fernando Sannibale,[2] James Nasiatka,[2] Mengjia Gaowei,[3] John Sinsheimer,[3] Erik Muller,[1] John Smedley,[3] and Howard Padmore[2]

[1]*Department of Materials Science and Engineering, Stony Brook University, Stony Brook, New York 11794, USA*
[2]*Lawrence Berkeley National Laboratory, Berkeley, California 94720, USA*
[3]*Brookhaven National Laboratory, Upton, New York 11973, USA*

(Received 2 September 2017; published 9 November 2017)

K-Cs-Sb bialkali antimonide photocathodes grown by a triple-element codeposition method have been found to have excellent quantum efficiency (QE) and outstanding near-atomic surface smoothness and have been employed in the VHF gun in the Advanced Photoinjector Experiment (APEX), however, their robustness in terms of their lifetime at elevated photocathode temperature has not yet been investigated. In this paper, the relationship between the lifetime of the K-Cs-Sb photocathode and the photocathode temperature has been investigated. The origin of the significant QE degradation at photocathode temperatures over 70 °C has been identified as the loss of cesium atoms from the K-Cs-Sb photocathode, based on the *in situ* x-ray analysis on the photocathode film during the decay process. The findings from this work will not only further the understanding of the behavior of K-Cs-Sb photocathodes at elevated temperature and help develop more temperature-robust cathodes, but also will become an important guide to the design and operation of the future high-field rf guns employing the use of such photocathodes.

DOI: 10.1103/PhysRevAccelBeams.20.113401

I. INTRODUCTION

APEX, the Advanced Photoinjector Experiment at Lawrence Berkeley National Laboratory (LBNL), is an operating injector test facility developed for characterizing the VHF gun, a new concept with high-brightness and high-repetition-rate radio-frequency (rf) gun designed to deliver free electron laser (FEL) quality electron beams at MHz repetition rate [1]. The mA-class current requirement for the gun imposes the use of high quantum efficiency (QE) semiconductor photocathodes if a realistic laser power is considered. Owing to its high QE, low emittance and a fast response time in the visible range, K-Cs-Sb has emerged as an excellent photocathode material for such high repetition-rate FEL applications which require mA range current requirements [2]. The use of these cathode materials has been successfully demonstrated in low field dc gun based photoinjectors designed to deliver several tens of mA currents [3]. However, these cathodes have two possible drawbacks when used in high repetition rate, moderate-high electric field rf guns like APEX: (1) the traditional recipe to prepare K_2CsSb photocathodes involves the deposition of a 10–30 nm of Sb film followed by sequential deposition of K and Cs, which usually creates a film with a rough surface that can dramatically raise the intrinsic emittance at the photocathode, making it problematic to use for low emittance applications in moderate to high cathode field photoinjectors, such as APEX [4]; (2) the QE of K-Cs-Sb cathodes is sensitive to vacuum conditions and the operating cathode temperature, which limits the operational lifetime of the cathode in rf guns.

Recently, it was shown that nearly atomically smooth films of K-Cs-Sb can be obtained by a triple-element codeposition recipe in which all three elements of K, Cs and Sb are evaporated simultaneously onto the substrate. This recipe yields cathodes with ∼5% QE at 532 nm and provides a better reproducibility compared to the traditional sequential deposition recipe. This solves the roughness related emittance growth issue and enables the use of these photocathode materials in high-field electron guns [4,5]. So far, over a dozen of K-Cs-Sb photocathodes prepared by the codeposition method have been employed in the APEX VHF gun and have successfully demonstrated operational capabilities required by high repetition-rate FELs like LCLS-II [6].

The other issue faced by these cathodes in high repetition-rate rf guns is the photocathode operational lifetime, which is usually defined by the time for the QE of the cathode to

Published by the American Physical Society under the terms of the Creative Commons Attribution 4.0 International license. Further distribution of this work must maintain attribution to the author(s) and the published article's title, journal citation, and DOI.

drop to $1/e$ of its initial value [7]. There are several factors that can reduce the lifetime of the alkali antimonide photocathode [8]. Due to their extreme sensitivity to chemical contaminations, the oxidizing residual gas species of H_2O, CO_2, O_2 and CO inside the growth chamber and the gun cavity can affect their lifetime [7]. Maintaining a clean UHV environment with total pressure controlled in the low 10^{-10} mbar range can minimize the effect of the gas contaminants on the lifetime [9]. Another crucial factor is the temperature of the photocathode during operation. The operational temperature of the photocathode can rise due to the tremendous rf power being dissipated in the walls of the cavity of an rf gun. For example, during the operation of the APEX VHF gun about 100 kW rf power is applied to the gun cavity, which generates a huge amount of heat. Even with the help of the effective water cooling system the temperature at the photocathode can increase by few tens of degrees Celsius above room temperature. Hence, it is important to measure the performance of the alkali antimonide photocathode at elevated temperatures to understand its behavior and operational lifetime in a VHF gun.

A previous study [10] on K-Cs-Sb photocathodes grown by traditional recipe has shown that their lifetime at 120 °C dropped by 3 orders of magnitude compared to that at room temperature, but the exact temperature at which the decay starts has not been measured. The triple-element codeposition creates a cathode with a smooth surface and possibly a different grain structure as compared to the traditional sequential deposition method. Hence, it is necessary to explore the robustness of the K-Cs-Sb photocathode grown by triple-element codeposition method and understand the QE degradation mechanism both in the growth chamber and in the operational VHF-gun environment at temperature elevated by few tens of degrees Celsius above the room temperature.

In this paper, we first report results of the cathode temperature and the performance of the K-Cs-Sb photocathode under the operational condition in the APEX VHF gun in Sec. II. In Sec. III, we present the results of the temperature-dependent lifetime measurement of K-Cs-Sb photocathodes grown by the triple-element codeposition method. Finally, we present results of *in situ* x-ray characterization, spectral response measurement and recesiation experiment throughout the decay process of the K-Cs-Sb photocathode to understand the mechanism for QE degradation at the elevated cathode temperature. These studies as an entity will provide a guidance regarding the optimal operation temperature of the K-Cs-Sb photocathode for its application in moderate-high gradient rf guns and shed light on the QE decay mechanisms at elevated temperatures, providing guidance to developing new cathode growth recipes for improved temperature robustness.

II. PHOTOCATHODE CONDITION IN THE APEX VHF GUN

A. Photocathode temperature

Figure 1 shows a cross section of the gun and its main components. The gun was fabricated and tested at LBNL, and based on its successful performance, a close version of the gun is being fabricated at LBNL to operate as the electron source for the LCLS-II, the high-repetition-rate x-ray FEL at SLAC [11]. The back wall of the gun is connected to a vacuum load lock system [12] that allows for the in-vacuum transfer of cathodes from the deposition chamber, located elsewhere, to the gun using a dedicated UHV vacuum "suitcase." The cathode material is deposited on a polished sintered molybdenum plug over a 1 cm diameter circular surface, which after insertion in the gun

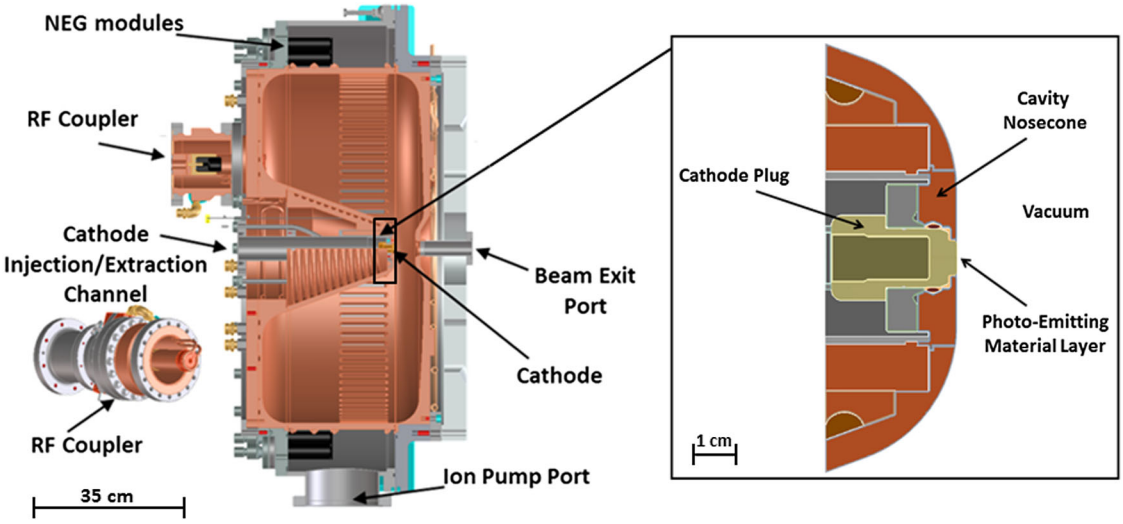

FIG. 1. Cross section of the APEX VHF gun with its main components in evidence. The inset shows the detail of the cathode plug area.

receptacle is exposed to the rf fields. The inset in Fig. 1 shows the detail of the cathode plug inserted in the gun nose cone.

At the nominal operation about 100 kW of rf power is dissipated on the gun cavity walls. The large majority of this power is removed by a water cooling system, and at equilibrium, the temperature of the different parts of the gun assumes a determined reproducible distribution. From the cathode material QE point of view, the relevant information is the operation temperature of the cathode plug because it can potentially be one of the main factors determining the QE lifetime in operation.

Radio frequency and mechanical constraints do not allow placing a temperature probe directly on the cathode plug, for this reason finite element analysis (FEA) was used for calculating the temperature of the part. ANSYS [13] simulations of the gun "nose cone" (where the plug is located) were performed using, as visible in the left part of Fig. 2, a refined mesh and exploiting the cylindrical symmetry of the gun to get the required accuracy while still maintaining a reasonable calculation time.

In order to accurately reproduce the experimental situation, operation parameters such as rf power, cooling water flows and temperatures were measured and used in the simulations. Figure 2 (right) shows the results of the analysis, indicating an operational temperature of the plug slightly above 45 °C. The simulation assumes a minor thermal conduction path between the plug and the cathode insertion arm. The magnitude of such conduction depends on the pressure that the arm exerts on the plug, the lesser the pressure the higher the temperature of the plug. In the worst-case scenario (negligible thermal conduction) the equilibrium value can rise to about 47.6 °C, which is the temperature of the adjacent nosecone part. For future VHF rf gun based photoinjectors that are designed for higher electric fields, more rf power will be needed and the photocathode temperature will be affected accordingly.

B. Photocathode performance

Over a dozen K-Cs-Sb photocathodes grown by co-deposition have been characterized in the APEX VHF gun. The overall performance of the photocathodes has been summarized below. For all the K-Cs-Sb photocathodes prepared at LBNL, no significant reduction of QE was recorded during the transfers from the preparation chamber to the vacuum suitcase, and from the vacuum suitcase to the gun. No enhancement of electron field emission (dark current) from the surface of the cathodes was measured. A cathode intrinsic emittance of 0.5–0.6 μm per mm rms was measured in the gun over several cathodes at 532 nm. This measurement agrees well with the previous intrinsic emittance measurements of K-Cs-Sb cathodes in dc guns [14]. No evidence of QE depletion in the cathode central area due to ion back-bombardment or heating or sputtering induced by the laser used for inducing photoemission from the cathode was found.

The $1/e$ QE lifetime of about three days in APEX was observed. During this period the gun was operational roughly 40% of the time. The QE decay rate during operational and nonoperational time was very similar with the rate during operational time being marginally higher. The QE decay was with reasonable approximation uniform over the cathode surface. Initial QE of these K-Cs-Sb photocathodes ranged between 2% to 5%. During operation the pressure in the gun was about 6–8 $\times 10^{-10}$ Torr with hydrogen being the dominant residual gas. Other atomic/molecular components (H_2O, O_2, CO, CO_2 and by-products) showed partial pressures always 1 to 2 orders of magnitude smaller than the total pressure. A fluorine partial pressure of about

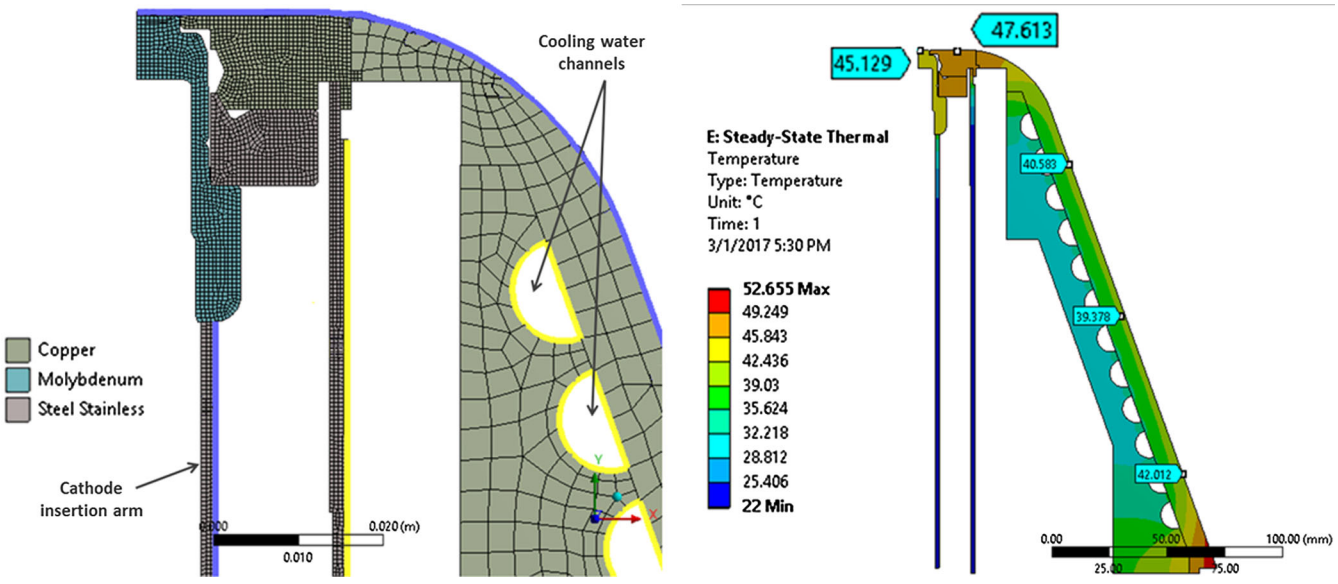

FIG. 2. Left: Detail of the fine mesh used for the FEA analysis. Right: FEA analysis results.

5×10^{-12} Torr was also present as the residual of an earlier contamination accident.

III. LIFETIME MEASUREMENT

In order to investigate the influence of the increased operating temperature on the relatively short (~3 days) lifetime of the cathodes in the APEX photoinjector, the decay rate of K-Cs-Sb was measured in the growth chamber at various cathode temperatures. In this section, we present the details of this measurement and discuss its implications on the operational lifetime of cathodes and design of future photoinjectors.

A. Experimental details

The experiment of lifetime measurement of K-Cs-Sb bialkali antimonide photocathode at various cathode temperatures was carried out in the Photocathode Lab in Lawrence Berkeley National Laboratory. A series of K-Cs-Sb photocathodes were prepared using the three-element deposition method, which is based on the growth recipe in Ref. [4]. In our experiments, phosphorus-doped N-type Si (100), of size 1 cm × 1 cm, were used as the substrate. The Si substrates were first cleaned in an ultrasonic acetone bath, followed by an ultrasonic isopropanol alcohol bath and then blown dry with nitrogen. In this paper, we assume that the degradation in QE is either due to temperature or chemical contaminants changing the surface and/or the bulk of the alkali-antimonide film and that the substrate (either Mo or Si) has no role to play as far as the QE degradation is concerned. After being transferred into the growth chamber, the substrates were heated up to 200 °C for one hour, which was sufficient to remove residual water on the surface. High purity Sb beads were installed into an Sb evaporator that was positioned at about 20 cm away from the sample. K and Cs dispensers purchased from the SAES Group [15] were used as alkali sources and were positioned at about 5 cm away from the sample. The substrate temperature was stabilized at about 80 °C prior to the growth. The Sb crucible was then heated up to 420 °C, K and Cs sources were turned on when the Sb crucible temperature was stabilized. The ratio of the evaporation rate of K and Cs was set at about 1:1 by controlling current through the sources. Partial pressure of all the major gas species including potassium and cesium was recorded by a residual gas analyzer. Typical total pressure in the growth chamber during deposition is kept in the mid-10^{-10} Torr range with a partial pressure of water in the 10^{-12} Torr range. During the growth, the photocurrent from the photocathode was monitored by Keithley 6517B electrometer [16]. The photocathode surface was illuminated by a 532 nm dc laser with a laser power of 0.44 mW for photocurrent measurement. The growth was terminated when the photocurrent stopped increasing at a typical QE of 4%–6%. The K and Cs sources are turned off after the Sb evaporator. The entire growth process usually takes 2–3 hours.

The as-grown photocathodes were heated at different temperatures for QE degradation measurements, which were performed by continuously shining the green laser onto the photocathode. A measurement at one temperature was done on one unique photocathode sample. The spectral response measurements were carried out before and after the decay using a laser-driven light source (Energetiq EQ1500) [17] and a stigmatic Czerny-Turner monochromator [18] with a resolution of about 1 nm. A step size of 2 nm was used for all the spectral response measurements.

In order to confirm that the observed decay was not due to the outgassing of the heater, the sample was moved from the heating position onto the transfer arm in the growth chamber. In this position the cathode is affected by the

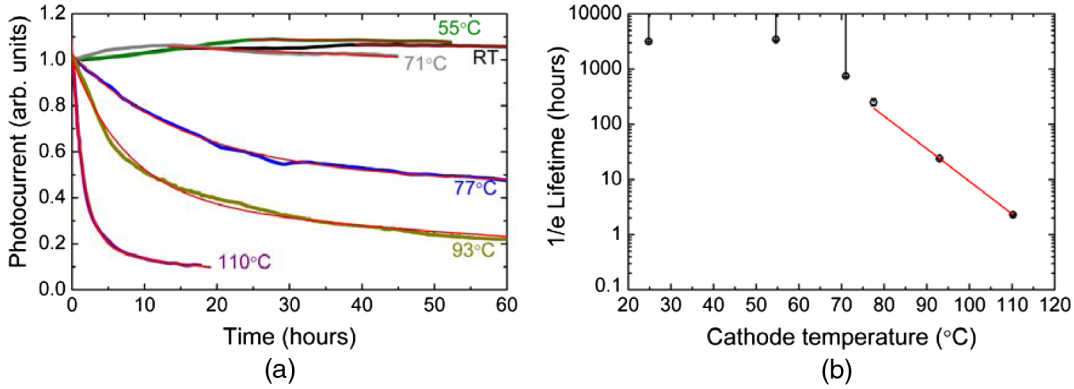

FIG. 3. (a) Decay curves of a series of K-Cs-Sb photocathodes at different temperature. The photocurrent was monitored by illuminating the cathode surface with a 532-nm laser. (b) 1/e lifetime of photocathodes as a function of different decay temperature. Due to the very large decay constants below 71 °C we indicate the 1/e lifetimes below these temperatures as the lower bounds for the lifetime. All other error bars of the estimated lifetime values that are calculated based on the 95% confident bounds of the fitted decay constants and amplitudes are within 10%, therefore smaller than the points. The red line is an exponential fit of 1/e lifetime data of 77 °C, 93 °C and 110 °C.

TABLE I. Decay constants and amplitudes from exponential fits with one term and two terms used for different sets of experimental data. The errors of all fitted parameters are within 10%.

	Exponential fit—first term		Exponential fit—second term	
Temperature (°C)	Decay constant (τ_1)	Amplitude (A_1)	Decay constant (τ_2)	Amplitude (A_2)
RT	3167	1.06	⋯	⋯
55	3443	1.08	⋯	⋯
71	741	1.05	⋯	⋯
77	761.9	0.51	15.7	0.52
93	114.3	0.39	7.63	0.61
110	28.8	0.18	1.65	0.85

heater outgassing without getting hot. A current of 8.4 A was passed through the heating filament for 12 hours. This current is sufficient to heat the sample to 110 °C if it was in the heating position. No QE decay was observed during these 12 hours, indicating that the outgassing from the heater is not significant enough to affect the decay measurements. Heater outgassing was also confirmed to be negligible from the measurements of the residual gas analyzer spectra before and during heating.

B. Results and discussions

Figure 3(a) shows the (at 532 nm wavelength of light) decay curves of a series of K-Cs-Sb photocathodes at different sample temperatures, with the initial photocurrent normalized to unity. To obtain the $1/e$ lifetime value from each measurement, exponential decay functions are used to fit the experimental data. In the lifetime measurements at room temperature (RT), 55 °C and 71 °C, the photocurrent gradually rises during the first 40 hours, 25 hours and 10 hours respectively before it starts to drop, hence the exponential fits are performed on the data points after the maximum photocurrent is reached. The experimental data at these decay temperatures is fitted by one exponential equation, $I_t = A_1 e^{-t/\tau_1}$, where I_t is the photocurrent after a certain length of time t, A_1 and τ_1 are the amplitude of the exponential decay and the decay constant. For the photocathodes decayed at 77 °C, 93 °C and 110 °C, a much faster photocurrent decay rate has been observed in the early stage of the experiment and it appears to slow down as the decay time increases. These decay curves can be better fitted by the double exponential equation, $I_t = A_1 e^{-t/\tau_1} + A_2 e^{-t/\tau_2}$, where A_2 and τ_2 are the second decay amplitude and decay constant.

All the exponential fits are shown as red lines in Fig. 3(a), from which the time needed for the photocurrent to drop to $1/e$ of the initial value can be calculated. At room temperature, the photocathodes grown by the three-element codeposition method generally have a $1/e$ lifetime of over 3000 hours. No significant QE degradation due to photocathode temperature is observed at the photocathode temperature of 55 °C, where the measured photocathode has a lifetime of over 3400 hours. The lifetime reduction becomes discernible at the decay temperature of 71 °C and higher. The $1/e$ lifetime from one exponential fit on the decay data at 71 °C is calculated to be 741 hours. For the photocathodes decayed at 77 °C, 93 °C and 110 °C, the time for their QE to drop to the $1/e$ of the initial value based on the two exponential fits are found to be roughly 225 hours, 24 hours, and 2.3 hours respectively. These lifetime values are plotted as a function of photocathode temperature in Fig. 3(b). As can be seen, an exponential drop in the lifetime regarding cathode temperature becomes prominent when cathode temperature exceeds 77 °C and an exponential fit to this range of data is marked as the red line.

The good agreement between the photocurrent decay curves at the higher temperatures and the double exponential fits indicates the coexistence of two decay mechanisms. The decay constants and the amplitudes of the exponential fits at different temperatures are listed in Table I for comparison. As the decay temperature increases from 77 °C to 110 °C, the first amplitude A_1 decreases and the second amplitude A_2 increases, furthermore, the first decay constant τ_1 is always more than an order of magnitude larger than the second decay constant τ_2. This indicates that the decay mechanism corresponding to A_2 and τ_2 that causes the fast decay at temperatures above 77 °C is suppressed at the lower temperatures, putting the threshold activation temperature for this decay mechanism between 71 °C and 77 °C.

The calculated temperature of the photocathode during operation based on the FEA analysis is below 50 °C, hence the temperature-induced QE degradation during the operation of the K-Cs-Sb photocathode would be very insignificant. The cause for the three-day operational lifetime of these photocathodes in the APEX gun could possibly be the chemical contamination (by fluorine) inside the gun cavity.

IV. DECAY PROCESS CHARACTERIZATION

So far we have demonstrated the temperature dependence of the lifetime of K-Cs-Sb photocathodes and their complex lifetime degradation behavior at different temperatures. To fully understand the decay mechanism, it is essential to obtain information on the chemical composition, crystal structure, spectral response and many other

properties of the photocathode throughout the decay process. In this section, we first show using x-ray fluorescence, diffraction and reflectivity measurements that the fast decay above 77 °C can be attributed to the loss of Cs from the cathode film. Then we show that it is possible to recover most of this loss by a straightforward recesiation process. We also present spectral response measurements to shed light on the decay process with longer decay time.

A. X-ray Characterization

In order to study the decay process, the QE degradation experiment was carried out in an *in situ* growth chamber at beam line G3 of the Cornell High Energy Synchrotron Source (CHESS), which has a photon energy of 11.24 keV ($\lambda = 1.103$ Å), following the same procedure as that used in LBNL. With the help of the specially designed growth chamber, *in situ* x-ray fluorescence (XRF), x-ray diffraction and x-ray reflectivity were recorded during the photocathode growth and decay process. Growth of K-Cs-Sb photocathodes was reproduced using the triple-element codeposition method. Pure metallic Sb beads were installed into a crucible and were used as the antimony source. K and Cs were evaporated from pure metal K and Cs ampoules that was installed into two separate pure alkali metal effusion cells. Deposition rates were checked by a quartz crystal microbalance that was placed alongside the sample. Growth temperature and deposition rates were controlled to be similar to that of the experiment performed at LBNL. Photocurrent was monitored by illuminating a 532-nm laser onto the photocathode, while simultaneously real-time x-ray fluorescence was recorded by a Vortex detector. The growth was terminated when the photocurrent reached the maximum, following the same criteria used in LBNL.

K-Cs-Sb photocathodes with similar QE at 532-nm wavelength as those grown at LBNL were reproduced in the beam line experiment. After the growth, the photocathode temperature was raised up to 100 °C to initiate the decay process. Photocurrent and x-ray fluorescence were recorded simultaneously during the decay process. The decay was terminated after the process was monitored for about 90 minutes while the QE decreased to 50% of the initial value after the growth. The lifetime of the photocathode decayed at 100 °C was calculated to be approximately 2.2 hours. Since the decay was measured only for 90 minutes, it could be fitted with only one exponential decay term corresponding to the quicker decay process. Hence, the decay constant of 2.2 hours corresponds to the decay constant of the quicker process only. This agrees well with the results obtained at LBNL. X-ray fluorescence, x-ray diffraction and x-ray reflectivity measurements were carried out before and after the decay by using a PILATUS 100 K 2D detector [19] to investigate the change in the composition, crystal structure, film thickness and surface roughness due to the decay process.

1. X-ray fluorescence

Figure 4 shows the x-ray fluorescence raw data and the fitted stoichiometry of the K-Cs-Sb photocathode before and after the decay [Fig. 4(a)], as well as the real-time atomic ratio of K:Sb and Cs:Sb of the film with error bars during the decay process [Fig. 4(b)]. The raw data is fitted by the program PyMCA [20]. The stoichiometry of the as-grown photocathode is found to be $K_{2.44}Cs_{0.6}Sb$, which turns out to be excessive in potassium and deficient in cesium compared to the targeted K_2CsSb. After the decay process which drops the QE by 50%, there appears to be no decrease in the potassium K_α and antimony L_α and L_β fluorescence peaks but only obvious drops in the cesium peaks including the two highest peaks of Cs L_α and L_β, as shown in Fig. 4(a). The real-time atomic ratio evolution for K:Sb and Cs:Sb during the decay also demonstrates that the photocathode continuosly loses cesium during the decay process. The final stoichiometry after the decay is fitted to

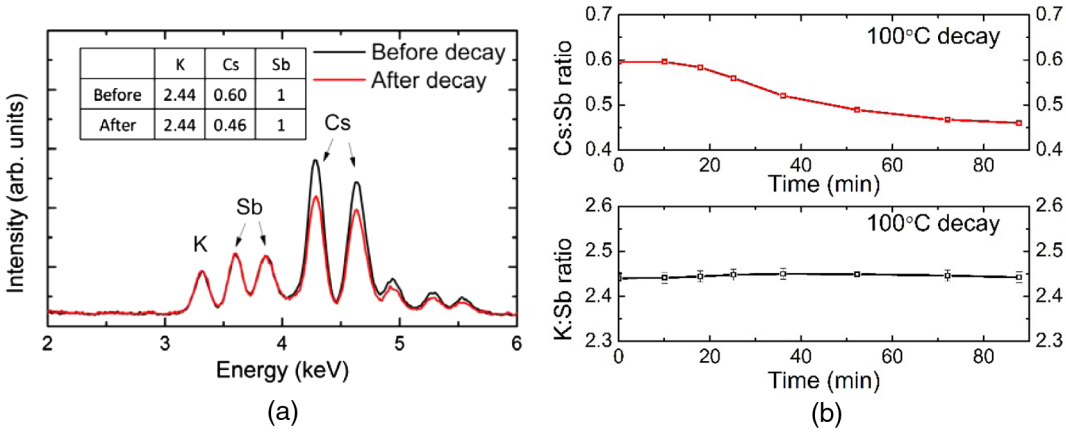

FIG. 4. (a) X-ray fluorescence results of the photocathode before and after the decay, the stoichiometry of the photocathode before and after the decay are shown in the inserted table. (b) Atomic ratio of K to Sb and Cs to Sb during the decay.

be $K_{2.44}Cs_{0.46}Sb$, which is clear evidence that the cesium depletion is the main cause for the K-Cs-Sb photocathode's QE degradation at 100 °C.

2. X-ray diffraction

The XRD scans were performed on the photocathode before and after the decay to investigate the change in the crystal structure; the details of the measurement can be found elsewhere [21]. The positions of the observed diffraction peaks, which are indexed based on the K_2CsSb crystal structure established in Ref. [22], before and after the decay are listed in Table II. A different grain structure has been observed based on the acquired diffraction pattern from the codeposited as-grown K-Cs-Sb photocathode which has a predominant (2 2 2) peak and weak (2 2 0) peak, when compared with the powder diffraction pattern acquired from polycrystalline K_2CsSb samples prepared by traditional recipe which has a predominant (2 2 0) peak [22,23]. Such a result is in good agreement with the previous study on the characterization of codeposited K-Cs-Sb photocathodes [5] and this indicates that a highly textured K-Cs-Sb thin film is formed by the codeposition method which contrasts with the polycrystalline film formed by the sequential deposition.

It has been observed that all the diffraction peaks are shifted to slightly higher 2θ values which indicates an average decrease of 0.31% in the lattice constant of the K-Cs-Sb crystals before and after the decay. Based on McCarroll's study [23], the K-Cs-Sb crystal lattice is expected to shrink as the bulk becomes more Cs deficient and K rich, which in our case is supported by the direct observation of the Cs depletion based on the XRF result. The peak intensities of the (222) and (220) peaks remain mostly identical which suggests the good integrity of the cubic crystal structure of the photocathode film. The intensity of the insignificant (111) peak increases by nearly an order of magnitude after the QE degradation, indicating conversion of the lattice from ordered K_2CsSb cubic structure to a disordered K-Cs-Sb cubic structure due to the Cs depletion from the lattice [23].

3. X-ray reflectivity

X-ray reflectivity (XRR) measurements were also performed before and after the decay process. The details of the measurement setup and data processing are given elsewhere [5]. The experimental and simulated XRR curves for the K-Cs-Sb photocathode before and after the decay are shown in Fig. 5, with the corresponding simulation results of each step that provide the best fit to the experimental data shown in Table III. It can be seen from the analyzed data that the final photocathode film after growth has a thickness of 54.1 nm, with observable oscillations up to $2\theta = 4°$. The simulation yields a rms roughness of 1.15 nm. The simulated thickness and roughness of the photocathode film grown by the three-element codeposition method are on a comparable level to those reported in a previous study [5]. After the decay is finished, the period of the XRR oscillations appears to be slightly larger, indicating a reduced film thickness. The simulation determines film thickness to be 51.6 nm, with an increased rms roughness of 1.39 nm, hence a reduction of 4.6% in the film thickness can be calculated after the decay.

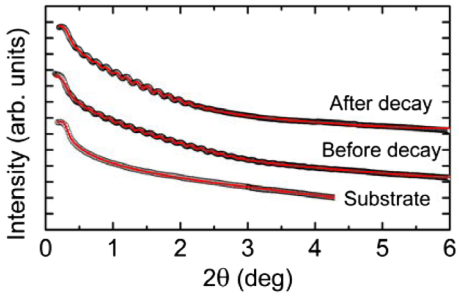

FIG. 5. X-ray reflectivity experimental data (circles) and simulated curves (red lines) of the K-Cs-Sb photocathode at different stages during the beam line experiment. The reflectivity intensity that was measured from the Si substrate, before-decay photocathode and after-decay photocathode, is demonstrated with an offset for clarity.

It should be noted again that the XRD analysis indicates the lattice size reduction of only 0.31%, which is much smaller than the total thickness reduction of 4.6%. This suggests that most of the Cs atoms released from the cathode during heating do not come from the lattice, but from a layer of excess Cs on the surface of the cathode or between the grain boundaries. Thus, it can be deduced that the main reason for the fast QE degradation of K-Cs-Sb photocathodes at elevated temperature is the depletion of surface Cs atoms that are not part of the lattice. The slower decay mechanism could not be studied using x-ray analysis due to the lack of time available at the x-ray beam line.

TABLE II. Diffraction peak positions obtained from the XRD scans performed on the photocathode before and after the decay.

Diffraction peaks	2θ position before decay	2θ position after decay
(1 1 1)	12.59°	12.62°
(2 2 0)	20.44°	20.51°
(2 2 2)	25.02°	25.11°

TABLE III. Simulation results to fit the XRR experimental data measured from the substrate and the photocathode before and after the decay. The simulation errors are shown in brackets.

Layer	Thickness (Å)	Roughness (Å)
After decay	516 (−4.49, 3.81)	13.9 (−0.10, 0.25)
Before decay	541 (−2.76, 4.02)	11.5 (−0.24, 0.63)
Substrate	⋯	2.35 (−0.01, 0.02)

B. Spectral response and recesiation process

Insight into the slower decay mechanism can be obtained by measuring the spectral response and by recesiating the decayed cathode to see whether the reduced QE can be recovered. For this purpose, two identical cathodes were grown at LBNL. One was heated to 110 °C for one hour and the other was heated to 110 °C for 12 hours. Upon completion of the heating, Cs was deposited on both cathodes while they were hot. Cs deposition rate during this recesiation process was identical to the Cs deposition rate during initial cathode growth.

The spectral responses over the range of wavelengths from 350 to 575 nm for the two photocathodes are shown in Figs. 6(a) and 6(b). In the case of one-hour decay in which the QE loss is mostly from the first exponential term of the fitted two exponential function, the recesiation step could renew the QE back to over 90% of the initial QE. In the 12-hour case where a larger contribution from the second term of the two exponential fit is expected, the recesiation step doubled the overall yield after the decay but could not return it to its former value, resulting in approximately 50% of the initial QE. Figures 7(a) and 7(b) show the ratio of the QE before decay to that after decay, as well as the ratio of the QE before decay to that after recesiation at different wavelengths for the two cathodes respectively. From these figures, it is clear that both photocathodes have undergone the largest reduction in QE in the long wavelength region, indicating an increase in the work function. The curve of the ratio between the QE before decay and after recesiation is nearly flat, indicating that the work function reaches the predecay value after recesiation.

These observations further support the claim that the fast decay is due to the loss of surface Cs which tends to increase the work function. Upon recesiation, this surface Cs layer is reformed reducing the work function back to its predecay value. This also suggests that mechanism for the longer decay does not change the work function and is not reversible by simply adding Cs. One possible mechanism that satisfies these criteria is the slow breakdown of the K-Cs-Sb lattice.

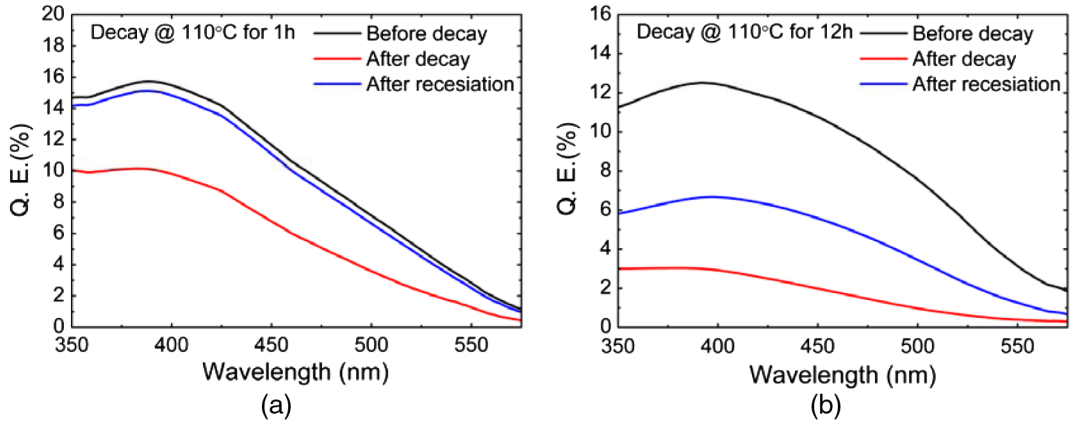

FIG. 6. Spectral response comparisons of the K-Cs-Sb photocathodes decayed at 110 °C for 1 hour (a) and 12 hours (b).

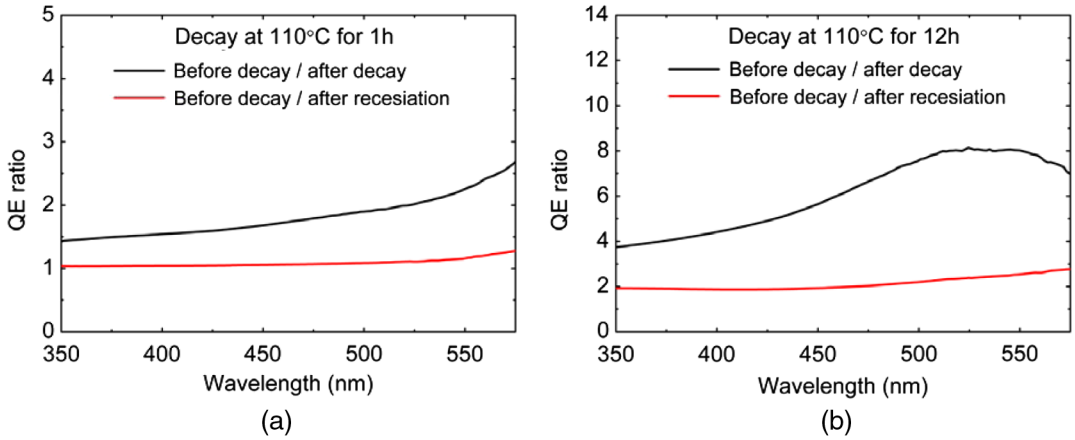

FIG. 7. Ratio of the QE before decay to the QE after decay and the ratio of the QE before the decay to after recesiation on photocathodes decayed at 110 °C for 1 hour (a) and 12 hours (b).

V. CONCLUSIONS

Studies on the temperature-dependent QE degradation of K-Cs-Sb photocathodes grown by three-element codeposition have been carried out at LBNL and CHESS. It has been found that these K-Cs-Sb photocathodes generally have a lifetime of over 3000 hours at room temperature in our growth chamber and still possess over 700 hours at a cathode temperature of 71 °C. No reduction in the lifetime has been observed up to a temperature of 55 °C. The cathode temperature in the APEX VHF gun was determined to be less than 50 °C. The temperature degradation measurements indicate that the K-Cs-Sb cathodes grown were stable up to 55 °C suggesting that the relatively short cathode lifetime (∼3 days) in this gun is not due to the temperature degradation of the cathode, but due to the chemical contamination (fluorine) in the gun. However, the QE degradation measurements presented acts as a guideline for the design of the future VHF gun which may operate at higher electric fields and result in higher cathode temperature.

Furthermore, the temperature-dependent decay of the K-Cs-Sb was studied using x-ray techniques and spectral response measurements. Above 77 °C the decay process was composed of two processes—a quick decay which can be attributed to the loss of Cs that was unreacted on the surface or between the lattice grains and a second slower decay that can possibly be explained by the slow degradation of the lattice. It may be possible to eliminate the quick decay of the cathode by growing a stoichiometrically correct K_2CsSb lattice by adjusting the deposition rates and substrate temperature during the codeposition based growth and ensuring that all Cs atoms have reacted. This could result in cathodes that are more robust to temperature.

ACKNOWLEDGMENTS

This work was supported by the Director, Office of Science, Office of Basic Energy Sciences of the U.S. Department of Energy, under Contracts No. KC0407-ALSJNT-I0013 and No. DE-AC02-05CH11231, and by the National Science Foundation under Grant No. Phy-1549132, the Center for Bright Beams.

[1] F. Sannibale *et al.*, Advanced photoinjector experiment photogun commissioning results, Phys. Rev. ST Accel. Beams **15**, 103501 (2012).

[2] T. Vecchione, I. Ben-Zvi, D. H. Dowell, J. Feng, T. Rao, J. Smedley, W. Wan, and H. A. Padmore, A low emittance and high efficiency visible light photocathode for high brightness accelerator-based X-ray light sources, Appl. Phys. Lett. **99**, 034103 (2011).

[3] L. Cultrera *et al.*, Photocathode behavior during high current running in the Cornell energy recovery linac photoinjector, Phys. Rev. ST Accel. Beams **14**, 120101 (2011).

[4] J. Feng, S. Karkare, J. Nasiatka, S. Schubert, J. Smedley, and H. Padmore, Near atomically smooth alkali antimonide photocathode thin films, J. Appl. Phys. **121**, 044904 (2017).

[5] Z. Ding, M. Gaowei, J. Sinsheimer, J. Xie, S. Schubert, H. Padmore, E. Muller, and J. Smedley, In-situ synchrotron x-ray characterization of K_2CsSb photocathode grown by ternary co-evaporation, J. Appl. Phys. **121**, 055305 (2017).

[6] F. Sannibale *et al.*, APEX Phase-II Commissioning Results at the Lawrence Berkeley National Laboratory, in *Proceedings of IPAC16, the 2016 International Particle Accelerator Conference, Busan, South Korea, 2016* (JACoW, Geneva, 2016), p. 1041.

[7] W. Anders, I. Bazarov, L. Cultrera *et al.*, *An Engineering Guide to Photoinjectors*, edited by D. H. Dowell and T. Rao (CreateSpace Independent Publishing Platform, 2013), ISBN-13: 978-1481943222, ISBN-10: 1481943227.

[8] D. H. Dowell, I. Barzarov, B. Dunham, K. Harkay, C. Hernandez-Garcia, R. Legg, H. Padmore, T. Rao, J. Smedley, and W. Wan, Cathode R&D for future light sources, Nucl. Instrum. Methods Phys. Res., Sect. A **622**, 685 (2010).

[9] A. di Bona, F. Sabary, S. Joly, P. Michelato, D. Sertore, C. Pagani, and S. Valeri, Development, operation and analysis of bialkali antimonide photocathodes for high-brightness photo-injectors, Nucl. Instrum. Methods Phys. Res., Sect. A **385**, 385 (1997).

[10] D. Dowell, S. Z. Bethel, and K. D. Friddell, Results from the average power laser experiment photocathode injector test, Nucl. Instrum. Methods Phys. Res., Sect. A **356**, 167 (1995).

[11] J. Galayda, The Linac Coherent Light Source-II Project, in *Proceedings of IPAC2014, the 2014 International Particle Accelerator Conference, Dresden, Germany, 2014* (JACoW, Geneva, 2014), p. 935.

[12] D. Sertore, S. Schreiber, K. Floettmann, F. Stephan, K. Zapfe, and P. Michelato, First operation of cesium telluride photocathodes in the TTF injector RF gun, Nucl. Instrum. Methods Phys. Res., Sect. A **445**, 422 (2000).

[13] Analysis System (ANSYS) software suite, www.ansys.com.

[14] I. Bazarov, L. Cultrera, A. Bartnik, B. Dunham, S. Karkare, Y. Li, X. Liu, J. Maxson, and W. Roussel, Thermal emittance measurements of a cesium potassium antimonide photocathode, Appl. Phys. Lett. **98**, 224101 (2011).

[15] See https://www.saesgetters.com/ for alkali metal dispensers.

[16] See https://www.tek.com/keithley-low-level-sensitive-and-specialty-instruments/keithley-high-resistance-low-current-electrom for Model 6517B.

[17] http://www.energetiq.com/DataSheets/EQ1500_Data_Sheet_.pdf.

[18] J. Feng, J. Nasiatka, J. Wong, X. Chen, S. Hidalgo, T. Vecchione, H. Zhu, F. Javier Palomares, and H. A. Padmore, A stigmatic ultraviolet-visible monochromator for use with a high brightness laser driven plasma light source, Rev. Sci. Instrum. **84**, 085114 (2013).

[19] See https://www.dectris.com/support/manuals-docs/pilatus/pilatus-2006-2013 for PILATUS 100K-S.

[20] V. A. Solé, E. Papillon, M. Cotte, Ph. Walter, and J. Susini, A multiplatform code for the analysis of energy-dispersive x-ray fluorescence spectra, A multiplatform code for the analysis of energy-dispersive X-ray fluorescence spectra, Spectrochim. Acta B Atom. Spectros. **62**, 63 (2007).

[21] M. Ruiz-Osés, S. Schubert, K. Attenkofer, I. Ben-Zvi, X. Liang, E. Muller, H. Padmore, T. Rao, T. Vecchione, J. Wong, J. Xie, and J. Smedley, Direct observation of bi-alkali antimonide photocathodes growth via in operando x-ray diffraction studies, Appl. Phys. Lett. Mater. **2**, 121101 (2014).

[22] K_2CsSb (CsK_2Sb) crystal structure: Data sheet from PAULING FILE Multinaries Edition—2012, in Springer materials http://materials.springer.com/isp/crystallographic/docs/sd_1215819.

[23] W. H. McCarroll, Chemical and structural characteristics of the potassium-cesium-antimony photocathode, J. Phys. Chem. Solids **26**, 191 (1965).